Sulym et al. Nanoscale Research Letters (2017) 12:152
DOI 10.1186/s11671-017-1935-x

Nanoscale Research Letters

NANO EXPRESS Open Access

Nanooxide/Polymer Composites with Silica@PDMS and Ceria–Zirconia–Silica@PDMS: Textural, Morphological, and Hydrophilic/Hydrophobic Features

Iryna Sulym[1*], Olena Goncharuk[1], Dariusz Sternik[2], Konrad Terpilowski[3], Anna Derylo-Marczewska[2], Mykola V. Borysenko[1] and Vladimir M. Gun'ko[1]

Abstract

SiO_2@PDMS and CeO_2–ZrO_2–SiO_2@PDMS nanocomposites were prepared and studied using nitrogen adsorption–desorption, Fourier transform infrared spectroscopy (FT-IR), scanning electron microscopy (SEM), measurements of advancing and receding contact angles with water, and microcalorimetry. The pore size distributions indicate that the textural characteristics change after oxide modification by poly(dimethylsiloxane) (PDMS). Composites are characterized by mainly mesoporosity and macroporosity of aggregates of oxide nanoparticles or oxide@PDMS nanoparticles and their agglomerates. The FT-IR spectra show that PDMS molecules cover well the oxide surface, since the intensity of the band of free silanols at 3748 cm^{-1} decreases with increasing PDMS concentration and it is absent in the IR spectrum at $C_{PDMS} \geq 20$ wt% that occurs due to the hydrogen bonding of the PDMS molecules to the surface hydroxyls. SEM images reveal that the inter-particle voids are gradually filled and aggregates are re-arranged and increase from 20 to 200 nm in size with the increasing polymer concentration. The highest hydrophobicity (contact angle $\theta = 140°$ at $C_{PDMS} = 20$–40 wt%) is obtained for the CeO_2–ZrO_2–SiO_2@PDMS nanocomposites. The heat of composite immersion in water shows a tendency to decrease with increasing PDMS concentration.

Keywords: Polymeric nanocomposites, Nanosilica@PDMS, CeO_2–ZrO_2–SiO_2@PDMS, Morphology, Textural characteristics, Hydrophobicity

Background

In recent decades, hydrophobic hybrid metal or metalloid oxide (MO)–polymer composites are widely used in a variety of applications such as self-cleaning hydrophobic coatings [1–3], chemical separation of polar and nonpolar substances [4, 5], adsorption of organic contaminants, and removal of oil from the water surface [6, 7]. The main attention is paid to development of film coatings and membranes [1–5, 8–12], as well as to highly dispersed materials with developed surface area [13–16]. To prepare highly dispersed hydrophobic composites, silica [13–15], titania [16, 17], zinc oxide [18], magnetic nanoparticles (γ-Fe_2O_3) [19], and mixed oxides [20–22] are often used. Highly dispersed composites with an adsorbed polymer layer on a nanoparticle surface are referred to core–shell nanocomposites (NC) [23] having a number of peculiarities. In NC with MO/poly(dimethylsiloxane) (PDMS) at a low polymer content, a major fraction of the polymer is located at the interfaces with nanoparticles [24–26]. The interfacial polymer fraction [25, 27] is characterized by a modified structure [28, 29], slower dynamics [30–33], and increased thermal stability [21] in comparison to the bulk. The use of complex MO cannot only improve the performance characteristics of the NC (such as thermal stability, durability [20, 21]) but also significantly affect their structural characteristics [20, 34]. The structure of the polymer adsorption layer defines such NC surface properties as hydrophilicity–hydrophobicity [34–36], compatibility with organics, adsorption capability, and reactivity [37–39]. The helix shape of PDMS with six Si–O

* Correspondence: sulim1981@mail.ru
[1]Chuiko Institute of Surface Chemistry, National Academy of Science of Ukraine, 17 General Naumov Street, 03164 Kiev, Ukraine
Full list of author information is available at the end of the article

bonds in a cycle [40] restricts the number of segments which can directly interact with a solid surface to form the hydrogen bonds SiO–H···O(Si(CH_3)$_2$–)$_2$. However, PDMS conformation can be changed in an adsorption layer depending on the PDMS content and MO structure (i.e., cores in the core–shell particles). A variation in the PDMS content can affect many properties of NC. Thus, such PDMS/zirconia/silica characteristics as the texture, hydrophobicity, and interfacial behavior strongly differ from those of PDMS/silica [19]. Therefore, the effects of structure of complex MO, as well as the impact of the content and molecular weight of PDMS, on the structural and hydrophobic properties of core–shell NC are highly relevant for further development and enhancement of core–shell NC with improved characteristics and regulated properties.

Upon creation of NC with MO/PDMS, a particular interest should be paid to complex MO, in which each component can enhance certain properties of the whole composite. Since the presence of such oxides as CeO_2 and ZrO_2 in MO/PDMS increases the thermal stability [21, 34, 41], the NC based on CeO_2–ZrO_2–SiO_2 could be a promising material. Preparation of similar complex nanooxides with a high specific surface was previously described in detail [42, 43].

Since the creation of the composites is primarily intended to obtain hydrophobic materials, the most important task is complete and correct characterization of their hydrophobic properties vs. structures. The hydrophobic properties of fine materials could be determined not only by measuring the contact angles [44, 45] but also by using a calorimetric technique to determine the heat of immersion in polar and nonpolar liquids [46, 47], and this method is optimal to evaluate the hydrophobicity of powder materials.

Thus, in the current study, the main attention is paid to the textural, morphological, and hydrophilic/hydrophobic properties of the polymer SiO_2@PDMS and CeO_2–ZrO_2–SiO_2@PDMS composites analyzed using SEM, adsorption, spectral, contact angle, and calorimetry methods.

Methods

Materials

Fumed silica (SiO_2) (pilot plant of the Chuiko Institute of Surface Chemistry, Kalush, Ukraine) and CeO_2–ZrO_2/SiO_2 were used as substrates for adsorption modification by poly(dimethylsiloxane). Silica-supported ceria–zirconia nanocomposites were prepared using a liquid-phase method and subjected to thermal treatment at 550 °C for 1 h. The content of grafted CeO_2 was 3 and 10 wt%, and the ZrO_2 content was constant at 10 wt% (CZS1 and CZS2, respectively). The synthesis and physicochemical characteristics of CeO_2–ZrO_2–SiO_2 nanooxides were described in detail previously [42, 43].

Commercial liquid poly(dimethylsiloxane) PDMS-400 ("Kremniypolimer", Zaporozhye, Ukraine, linear, –CH_3 terminated; molecular weight $W_m \approx 5700$, degree of polymerization $d_p = 75$) was adsorbed onto silica and ceria–zirconia–silica to prepare samples containing 5, 10, 20, and 40 wt% of the polymer. Before the adsorption, oxide samples were dried at 110 °C for 1 h, and then a solution of PDMS (1 wt%) in hexane was added and the suspension was stirred. The suspension was dried at room temperature for 24 h and then at 80 °C for 3 h. All samples with PDMS were in the powder form similar to the initial silica. The composition and textural characteristics of the NC are listed in Table 1.

Textural Characterization

To analyze the textural characteristics of initial oxides and oxide@PDMS nanocomposites, low-temperature (77.4 K) nitrogen adsorption–desorption isotherms were recorded using an ASAP 2405N (Micromeritics Instrument Corp., USA) adsorption analyzer after outgassing the samples at 110 °C for 2 h in a vacuum chamber. The values of the specific surface area (S_{BET}) were calculated according to the standard BET method [48]. The total pore volume V_p was evaluated from nitrogen adsorption at $p/p_0 = 0.98–99$ (p and p_0 denote the equilibrium and saturation pressures of nitrogen at 77.4 K, respectively). The nitrogen desorption data were used to compute the pore size distributions (PSD, differential $f_V \sim dV_p/dR$ and $f_S \sim dS/dR$) using a self-consistent regularization (SCR) procedure under nonnegativity condition ($f_V \geq 0$ at any pore radius R) at a fixed regularization parameter $\alpha = 0.01$ with voids (V) between spherical nonporous nanoparticles packed in random aggregates (V/SCR model) [49]. The differential PSD with respect to the pore volume $f_V \sim dV/dR$, $\int f_V dR \sim V_p$ were re-calculated to the incremental PSD (IPSD) at $\Phi_V(R_i) = (f_V(R_{i+1}) + f_V(R_i))(R_{i+1} - R_i)/2$ at $\Sigma\Phi_V(R_i) = V_p$. The f_V and f_S functions were also used to calculate contributions of micropores (V_{micro} and S_{micro} at $0.35\ nm < R < 1\ nm$), mesopores (V_{meso} and S_{meso} at $1\ nm < R < 25\ nm$), and macropores (V_{macro} and S_{macro} at $25\ nm < R < 100\ nm$).

Fourier Transform Infrared Spectroscopy (FT-IR)

FT-IR spectra of powdered samples (ground with dry KBr at the mass ratio 1:9) were recorded over the 4000–400 cm^{-1} range using a ThermoNicolet FT-IR spectrometer with a diffuse reflectance mode. For quantitative analysis, some IR spectra were normalized using the intensity of the Si–O vibration overtone at 1865 cm^{-1} as an inner standard.

Scanning Electron Microscopy (SEM)

The particulate morphology was analyzed using field emission scanning electron microscopy employing a QuantaTM 3D FEG (FEI Company, USA) apparatus operating at the voltage of 30 kV.

Table 1 Textural characteristics of initial oxides and oxide@PDMS nanocomposites

Sample	S_{BET} (m^2/g)	S_{micro} (m^2/g)	S_{meso} (m^2/g)	S_{macro} (m^2/g)	V_{micro} (cm^3/g)	V_{meso} (cm^3/g)	V_{macro} (cm^3/g)	V_p (cm^3/g)	$R_{p,V}$ (nm)
SiO_2	283.4	21.0	224.9	37.5	0.008	0.348	0.569	0.925	29
SiO_2@P5	224.8	27.1	131.9	65.8	0.002	0.054	2.168	2.224	29
SiO_2@P10	184.4	6.2	117.3	60.9	0.004	0.612	1.250	1.866	28
SiO_2@P20	149.2	4.1	85.6	59.5	0.003	0.638	1.152	1.793	27
SiO_2@P40	73.9	2.2	49.6	22.1	0.000	0.027	0.925	0.952	36
CZS1	250.8	23.2	146.7	80.9	0.007	0.067	1.257	1.331	54
CZS1@P5	204.8	32.0	139.8	33.0	0.018	0.678	0.703	1.399	26
CZS1@P10	165.0	2.7	117.6	44.7	0.000	0.040	1.290	1.330	29
CZS1@P20	130.6	4.2	97.6	28.8	0.003	0.522	0.585	1.110	27
CZS1@P40	63.0	4.1	26.4	32.5	0.002	0.080	0.668	0.75	40
CZS2	258.9	14.2	158.3	86.4	0.004	0.073	1.353	1.430	55
CZS2@P5	201.3	30.2	144.6	26.5	0.017	0.729	0.549	1.295	23
CZS2@P10	156.2	19.2	123.8	13.2	0.004	0.357	0.557	0.918	22
CZS2@P20	119.8	4.7	42.9	72.2	0.006	0.561	0.330	0.897	38
CZS2@P40	57.9	6.8	35.9	15.2	0.001	0.048	0.333	0.382	28

Specific surface area in total (S_{BET}) and of nanopores (S_{micro}), mesopores (S_{meso}), macropores (S_{macro}), and respective specific pore volumes (V_p, V_{micro}, V_{meso}, V_{macro}). $R_{p,V}$ represents the average pore radius determined from the differential pore size distributions with respect to the pore volume

Contact Angle Measurements

A Digidrop GBX Contact Angle Meter (France) equipped with a video camera and firm software was used in the contact angle (CA, θ) measurements. Using the tilting plate method, the contact angles were measured on the pressed (180 bars for 15 min) plates of samples inclined toward the optical axis and in that position liquid gathered on one side of the droplet and retracted on the other one. A 6-μl droplet [50] was set in a chamber in front of the Contact Angle Apparatus camera and then using a small table. The droplet was tilted at an appropriate angle. The whole process was filmed until it started to slide. The advancing contact angle (ACA) was measured just before the droplet sliding on the droplet front and the receding (RCA) on its rear. The values of CA were evaluated for both sides of the sample plate using the Win Drop++ program. To obtain the averaged CA values, the measurements were performed for 10 water droplets put on each sample. The measurements were conducted at 20 °C and humidity RH = 50%.

Apparent Surface Free Energy Determination

The apparent surface free energy of given surfaces was calculated using the contact angle hysteresis (CAH):

$$\gamma_s = \frac{\gamma_L(1+\cos\theta_a)^2}{2+\cos\theta_r+\cos\theta_a} \quad (1)$$

where γ_S is the apparent surface free energy, γ_L is the water surface tension (72.8 mJ/m^2 at 20 °C), θ_a is the advancing contact angle, and θ_r is the receding contact angle of water [51].

Microcalorimetry

Microcalorimetric investigation of oxides and composites was carried out using a DAC1.1A (Chernogolovka, Russia) differential automatic calorimeter. Before the measurements of the heat of immersion of samples in polar (water) or nonpolar (*n*-decane) liquids, the samples were degassed at 130 °C and 0.01 Pa for 2 h and then used (100 ± 5 mg per 3 ml of wetting liquid) without contact with air. Since the total heat of immersion depends on the mass and surface area of a sample, the obtained results were normalized to both 1 g of a sample and 1 m^2 of the surface area. To obtain the averaged Q values, the measurements were performed two to three times for each system and the average errors were ≤7%.

Results and Discussion

Textural Characteristics

The nitrogen adsorption–desorption isotherms for the initial oxides and composites (Fig. 1) display a sigmoidal-shaped course (type II of the IUPAC classification) with a narrow hysteresis loop of the H3 type [48, 52] in the p/p_0 range between 0.8 and 1.0. This indicates the formation of aggregates with the initially nonporous nanoparticles that are characterized by the textural porosity.

The incremental pore (voids between nonporous nanoparticles in aggregates) size distribution functions (Fig. 2) show that the textural characteristics change after the silica modification and the formation of polymeric–nanooxide composites.

The specific surface area (Table 1, S_{BET}) does not demonstrate a significant reduction after grafting of

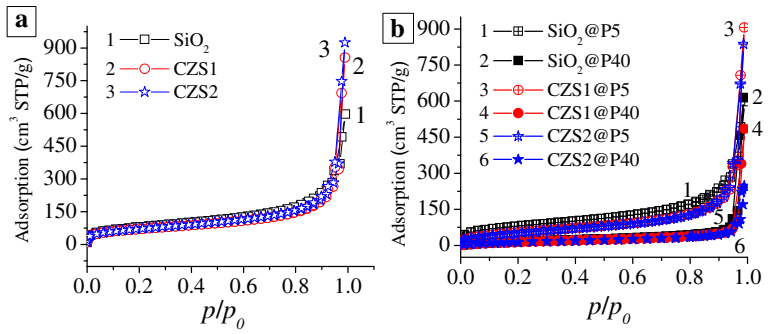

Fig. 1 Nitrogen adsorption–desorption isotherms of oxides **a** before and **b** after adsorption of PDMS

ceria–zirconia. All oxide samples (Fig. 2a) are mainly mesoporous (aggregates of SiO_2 nanoparticles) and macroporous (aggregates of modified SiO_2). In general, the average pore radii (Table 1, $R_{p,V}$) are by almost twice larger in CZS1 and CZS2, as compared to unmodified silica. The textural characteristics of the materials change due to the adsorption of PDMS (Table 1 and Fig. 2b). The values of S_{BET} of all composites decreased with the increasing polymer content by 74, 75, and 78% (in comparison to the initial oxides) for SiO_2@P40, CZS1@P40, and CZS2@P40, respectively, after the PDMS adsorption in the amount of 40 wt% (Table 1). The polymer adsorption leads to suppression of the pore volume (V_p) as well as V_{meso} and V_{macro}. After addition of PDMS, the average pore radii (Table 1, $R_{p,V}$) decrease. In general, the addition of polymer can change the porosity characteristics because each long macromolecule can be able to bind several oxide nanoparticles and their aggregates in more compacted structures. This leads to the decrease in the volume of voids between particles [53].

Fourier Transform Infrared Spectroscopy (FT-IR)

Adsorption modification of initial silica and CeO_2–ZrO_2–SiO_2 nanooxides was conducted with poly (dimethylsiloxane) due to the formation of hydrogen bonds $\equiv M_iO–H\cdots O(Si(CH_3)_2–)_2$ (where M = Si, Ce, or Zr, i = 1 or 2) between the oxygen atoms in the PDMS polymer chain and hydrogen atoms of the surface hydroxyls (–OH) of the oxide particles.

Figure 3 shows the FT-IR spectra in the region from 1000 to 4000 cm^{-1} for the initial oxides and oxide@PDMS composites. The broad band of high intensity at 3050–3700 cm^{-1} centered at 3300 cm^{-1} corresponds to the O–H stretching vibrations of surface hydroxyls and adsorbed water [54]. The peak located at 1628 cm^{-1} represents the bending vibrations of adsorbed water [55]. The FT-IR spectra intensity in the region of O–H vibrations gradually decreases with polymer adsorption. This suggests that a significant amount of the surface hydroxyls was disturbed by the PDMS chains and the amount of adsorbed water decreases. The FT-IR spectra show that for SiO_2@P20 and CZS2@P20 (Fig. 3a, b, curves 4), the band of the OH-stretching vibrations of free silanols at ν_{OH} = 3748 cm^{-1} does not occur.

The symmetric and asymmetric C–H stretching vibrations of the methyl groups of PDMS are observed at 2906 and 2963 cm^{-1} (Fig. 3), respectively, along with the deformation vibrations of the same groups at 1263 and 1406 cm^{-1} [56]. The peak intensity depends monotonically on the amount of adsorbed polymer.

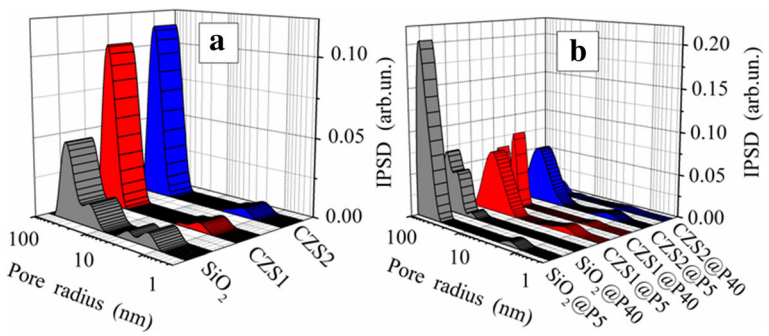

Fig. 2 Incremental pore size distributions of oxides **a** before and **b** after adsorption of PDMS

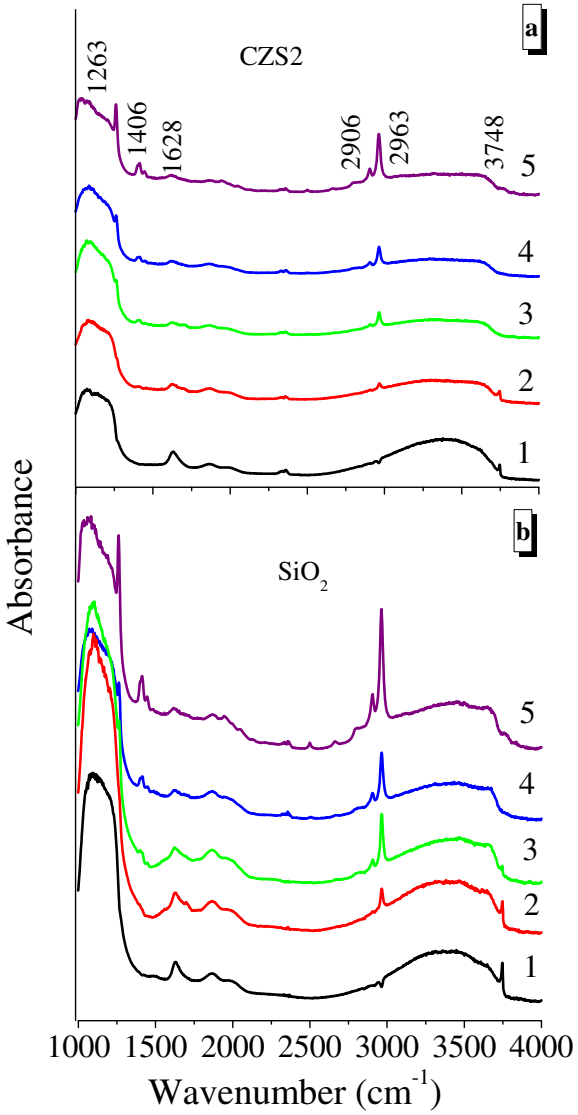

Fig. 3 FT-IR spectra of initial oxides and oxide@PDMS nanocomposites for (**a**, curve 1) CZS2 and (**b**, curve 1) SiO_2 at C_{PDMS} 5 wt% (**a**, **b** curves 2), 10 wt% (**a**, **b** curves 3), 20 wt% (**a**, **b** curves 4), and 40 wt% (**a, b** curves 5)

Scanning Electron Microscopy

SEM images (Fig. 4) show changes in the outer surfaces of samples due to the adsorption of PDMS. For the composites with PDMS, a significant increase in aggregate sizes is observed, but structure of composites remained dispersed even at C_{PDMS} = 40 wt%. A tendency to increase the size of aggregates with the increasing PDMS concentration takes place for all samples. The structure of the initial oxides corresponds to small aggregates with a disordered loose structure. Thus, for SiO_2, CZS1, and CZS2, the size of aggregates is 10–20 nm; upon their modification with 5 wt% PDMS, the aggregate size became from 20 to 40 nm; and when the amount of PDMS is 40 wt%, the aggregate size increases to 70–200 nm. For all composites, the polymer forms a shell of nanoparticles. The remained powder texture of oxide@PDMS composites similar to that of the initial oxide powders suggests well distributed PDMS molecules at the surfaces of all nanoparticles. A uniform coating of the oxide particles by PDMS layer occurs due to stronger interactions of PDMS with the oxide surface than with the other polymer macromolecules.

Additionally, according to [34], the average thickness of a PDMS layer was calculated. The obtained results (Table 2) show that this value depends weakly on the type of oxide composition studied. It depends mainly on the amount of PDMS. This weak influence of the particle composition is due to a relatively low content of CeO_2 and ZrO_2, i.e., the particulate morphology is mainly determined by the silica matrix. Taking into account aggregation of nanoparticles, one can assume that these values of h are minimal of possible ones. In other words, the maximal thickness of the PDMS layer could be larger, at least, by a factor of 1.3–1.5 than the average one. However, a contact zone between adjacent oxide nanoparticles in aggregates could be free of PDMS or covered by a monomolecular layer independent of the total amounts of PDMS.

Hydrophilic/Hydrophobic Properties of Composites

Surface wettability is one of the research hotspots in surface science. Lately, hydrophobic surfaces, especially superhydrophobic surfaces, have attracted considerable attention because of their extensive applications in self-cleaning, biomaterials, droplet transportation, etc.

Evaluation of the hydrophobic properties of the composites was carried out by measurements of the contact angle of wetting with water. The apparent surface free energy (γ_S) was determined using the ACA/RCA hysteresis approach [51].

The water contact angle measurement demonstrated that the hybrid CeO_2–ZrO_2–SiO_2@PDMS surfaces (Fig. 5b, c) are much more hydrophobic than SiO_2@PDMS (Fig. 5a) even at small amounts (10 wt%) of the polymer. However, all NC are hydrophilic at $C_{PDMS} \le 5$ wt%. The values of ACA and RCA depend on the nature of the oxide matrix and polymer concentration.

The surface free energies are significantly higher for SiO_2@PDMS than for CeO_2–ZrO_2–SiO_2@PDMS composites (Fig. 6). It was found that the surface free energies extremely decreased from 30.8 ± 3.2 mJ/m^2 to 7.6 ± 1.3 mJ/m^2 for the SiO_2@PDMS composites with the increasing amount of PDMS while for the CZS samples, this value hardly changes. Indeed, stronger changes in the interaction of composites with water occur before the PDMS monolayer formation because the interactions of oxide surface (hydrophilic) and PDMS (hydrophobic) with water differ largely.

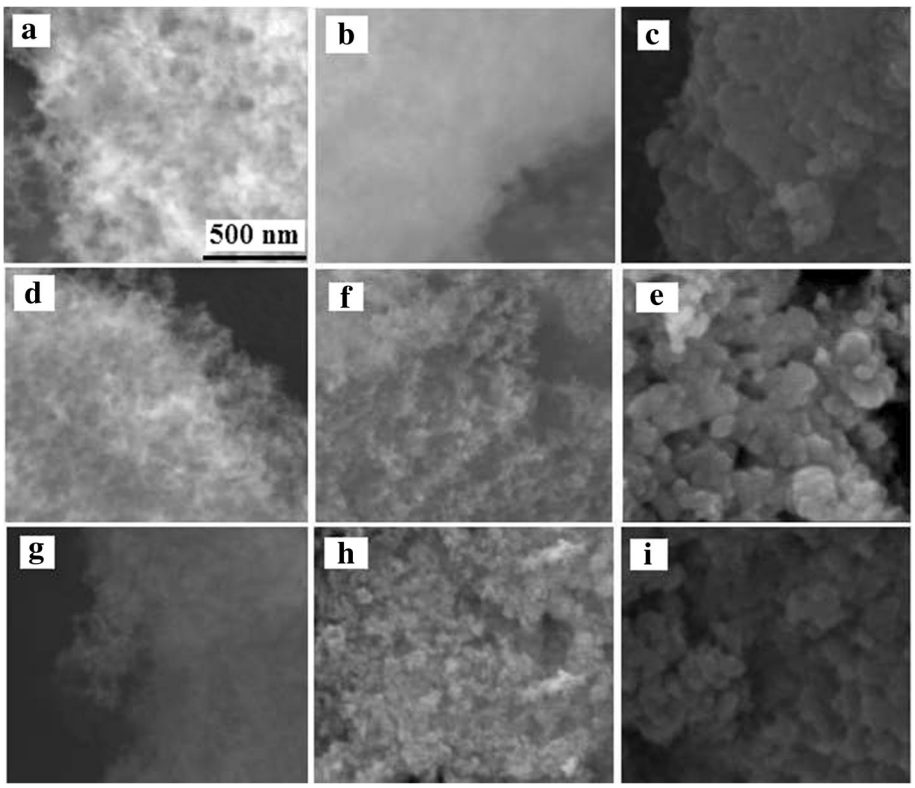

Fig. 4 SEM images (the *scale bar* is 500 nm) of the initial oxides and oxide@PDMS nanocomposites. **a** SiO_2. **b** SiO_2@P5. **c** SiO_2@P40. **d** CZS1. **f** CZS1@P5. **e** CZS1@P40. **g** CZS2. **h** CZS2@P5. **i** CZS2@P40

Interactions of Composites with Polar (Water) and Nonpolar (Decane) Liquids

Conditions of interactions of water with composites in the microcalorimetry method differ from those measuring the CA by a lack of the gas phase, which affects the wetting. The Gibbs free energy of the system decreases upon immersion of a composite into a liquid. This occurs due to compensating high surface energy of a solid surface interacting with a liquid that is accompanied by the heat release [57].

Table 2 Average diameter (*d*) of uncoated and coated nanoparticles and average thickness (*h*) of the PDMS layer

Sample	*d* (nm)	*h* (nm)
SiO_2	9.62	
SiO_2@P10	15.7	3.0
SiO_2@P40	47.6	19.0
CZS1	8.87	
CZS1@P10	14.4	2.8
CZS1@P40	47.5	19.3
CZS2	7.85	
CZS2@P10	13.5	2.8
CZS2@P40	46.8	19.5

According to the molecular theory of wetting [58], interfacial energy is considered as a measure of the balance of dispersive and polar intermolecular interactions, and the contributions of these interactions are additive. Depending on the nature of the solid surface and liquid interacting with it, the relationship between the polar and nonpolar interactions will determine the heat of immersion [59, 60].

The heats of immersion in water (Q_w) and decane (Q_d) calculated per 1 g of SiO_2@PDMS and CeO_2–ZrO_2–SiO_2@PDMS nanocomposites at different C_{PDMS} are given in Table 3. Comparison of the heats of immersion of the oxides without PDMS showed that the modification of the SiO_2 with Ce- and Zr-oxides results in increasing the heat of immersion in water, while the heats of immersion in decane are almost unchanged (Table 3). This indicates that CeO_2–ZrO_2 can enhance the surface hydrophilicity due to the formation of new active centers of the hydrophilic nature such as OH groups and bridge M–O(H)–M bonds.

After modification of nanooxides with PDMS the surface hydrophilic active centers forming the hydrogen bonds with PDMS become less accessible or inaccessible for water molecules. For all composites SiO_2@PDMS and CeO_2–ZrO_2–SiO_2@PDMS, the heats of immersion

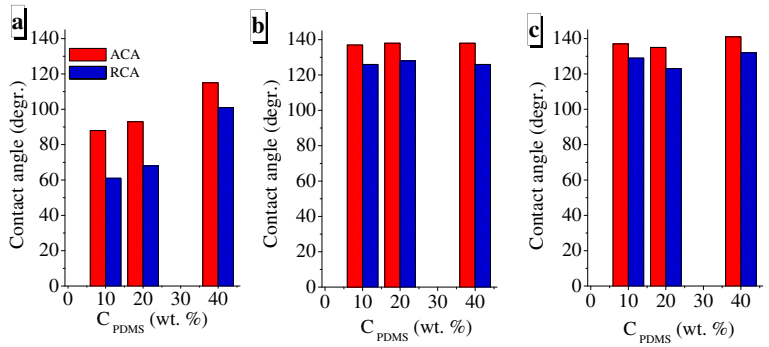

Fig. 5 Contact angle measurements on the surface of **a** SiO_2@PDMS, **b** CZS1@PDMS, and **c** CZS2@PDMS nanocomposites

in water significantly decrease with the increasing PDMS content. In general, the heat of immersion in water is determined by the total value of wetted composite surface, the structure of adsorbed PDMS surface layer and accessibility of oxide surface for interactions with the wetting liquid. Therefore, the decrease in the heat of immersion in water can be attributed to two factors: (i) reduction of specific surface of composites with the increasing PDMS content, and (ii) changes in the structure of the surface layer interacting with water.

To exclude the effect of specific surface area and to determine precisely the contribution of the surface structure to the polar and nonpolar interactions, the heats of immersion in water and decane were recalculated per 1 m^2 (Fig. 7). In the range of PDMS concentrations prior to the formation of a monolayer on the CeO_2–ZrO_2–SiO_2 surface (10–15 wt%), a sharp decrease in the immersion heat in water is observed with the increasing PDMS content. However, with a further increase in the content of PDMS, some increase in the heat of immersion in water was manifested, though CA displayed high values (Fig. 5) that defined these samples as hydrophobic. The heats of immersion in decane correlated with the values of the specific surface area; therefore, their increase for the samples with a high PDMS content was not observed (Fig. 7, Table 1). This peculiarity can be explained by the fact that the structure of the adsorbed layer strongly depends on the content of PDMS in the composite. Since during adsorption the polymers are always associated and form supramolecular structures, the structure of the adsorbed layer depends on the polymer content in the system: with the increasing polymer content PDMS macromolecules form the primary and secondary supramolecular structures, for which bonds with the solid surface may be weaker than that for flat-adsorbed molecules. At a low content, PDMS forms the adsorption layer with a flat structure, in which a maximal interaction of macromolecules with the surface active sites is implemented, and the water molecules do not have access to interact with hydrophilic active centers of nanooxides. While at a high content of PDMS, macromolecules form loops, tails, and assemblies with each other and such polymer structures can be more mobile than the flat ones during the contact with water access to the interactions of water molecules with the surface active centers of complex oxides without air absence and water excess because interaction of water with PDMS is thermodynamically unfavorable. Thus, the wetting of the composites surface depends on the structure of

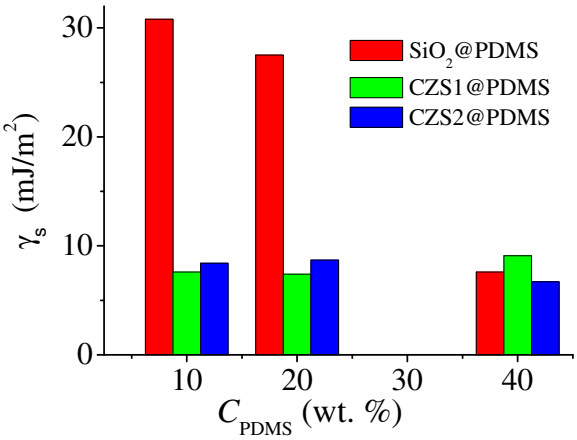

Fig. 6 Apparent surface free energy calculated from the hysteresis (CAH) approach

Table 3 The heat of immersion in water and decane liquids for the SiO_2@PDMS and CeO_2–ZrO_2–SiO_2@PDMS composites

C_{PDMS} (wt%)	SiO_2		CZS1		CZS2	
	Q_w(J/g)	Q_d(J/g)	Q_w(J/g)	Q_d(J/g)	Q_w(J/g)	Q_d(J/g)
0	41.2	20.5	57.7	22.3	60.2	19.5
5	28.1	13.4	33.9	10.8	35.9	11.6
10	13.3	5.1	11.8	7.3	13.1	7.9
20	11.9	6.1	10.7	6.1	11.5	5.3
40	3.0	2.2	6.8	4.2	8.7	1.8

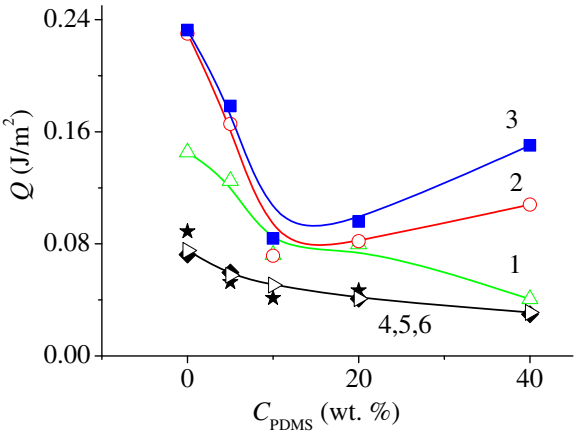

Fig. 7 The dependence of the heat of immersion in water (*1*, *2*, *3*) and decane (*4*, *5*, *6*), normalized to 1 m^2, on the content of PDMS composites: SiO_2@PDMS (*1*, *4*), CZS1@PDMS (*2*, *5*), and CZS2@PDMS (*3*, *6*)

the adsorption layer of PDMS which changes with the increasing content of PDMS and the polar or nonpolar nature of the wetting fluid.

Conclusions

Nanooxides (SiO_2 and CeO_2–ZrO_2/SiO_2) were used as substrates for adsorption modification by PDMS-400 in the amounts of 5, 10, 20, and 40 wt%. Effects of nanostructured oxides on the textural and morphological characteristics of polymer silica@PDMS and ceria–zirconia–silica@PDMS NC were studied employing structure (adsorption–desorption nitrogen isotherms, FT-IR) and morphology (SEM) techniques. Microcalorimetry and measurements of the contact angle of wetting with water were performed to investigate the hydrophobic properties of the materials.

It was found that the specific surface area of nanooxide@PDMS composites decreases with the increasing C_{PDMS}, and this decrease is larger for the CZS@PDMS systems. In general, the polymer adsorption leads to decrease in the values of V_p, V_{meso}, and V_{macro} as well as $R_{p,V}$. The analysis of the FT-IR spectra shows that all surface OH groups of oxides are disturbed due to the interactions with PMDS and adsorbed water.

The SEM images showed that the composites retain in the disperse state at the concentration of 5–40 wt% PDMS, and they can be considered as core–shell nanocomposites due to the well-distributed PDMS molecules at the surfaces of all nanoparticles of oxides.

The nanocomposites displayed high values of the main parameters related to the hydrophobicity (ACA and RCA). The contact angles of water drops for the complex oxide with adsorbed PDMS are about 140° at C_{PDMS} = 10–40 wt% while for the SiO_2@PDMS composites it is of 120°. It was found that the surface free energies extremely decreased from 30.8 ± 3.2 mJ/m^2 to 7.6 ± 1.3 mJ/m^2 for SiO_2@PDMS composites with the increasing amount of PDMS, while for ceria–zirconia–silica systems, this value is low ($\leq 9.1 \pm 1.3$ mJ/m^2) at any content of PDMS.

The heats of immersion in water significantly decrease with increasing PDMS content in the composites due to two factors: formation of the hydrogen bonds between the hydrophilic active sites of oxides and PDMS leading to the decrease in their accessibility to the interactions with the water molecules and reduction of the specific surface area of composite with the increasing PDMS concentration. However, at a high content of polymer (40 wt%), the interactions of composites with water can increase due to higher aggregation of PDMS molecules each other resulting to the adsorbed layer structure changes.

Thus, this study presents promising results for an easy and cost-effective alternative using such composites as protective coatings with appropriate hydrophobic properties.

Acknowledgements

The authors are grateful to the European Community, Seventh Framework Programme (FP7/2007–2013), Marie Curie International Research Staff Exchange Scheme (IRSES grant no 612484) for financial support of this work. The research was partly carried out with the equipment purchased, thanks to the financial support of the European Regional Development Fund in the framework of the Polish Innovation Economy Operational Program (contract no. POIG.02.01.00-06-024/09 Center of Functional Nanomaterials).

Authors' Contributions

IS carried out the synthesis and characterization of the nanocomposites by the FT-IR method. DS and ADM participated in the SEM and nitrogen adsorption–desorption studies. KT participated in the contact angle measurements for polymer composites as well as calculated the apparent surface free energy. OG carried out the microcalorimetric investigations of nanocomposites. OG and IS analyzed the data and drafted the manuscript. VMG, MVB, and ADM revised the manuscript. All authors read and approved the final manuscript.

Competing Interests

The authors declare that they have no competing interests.

Author details

[1]Chuiko Institute of Surface Chemistry, National Academy of Science of Ukraine, 17 General Naumov Street, 03164 Kiev, Ukraine. [2]Department of Physicochemistry of Solid Surface, Faculty of Chemistry, Maria Curie-Sklodowska University, M. Curie-Sklodowska Sq. 3, 20-031, Lublin, Poland. [3]Department of Interfacial Phenomena, Faculty of Chemistry, Maria Curie-Sklodowska University, M. Curie-Sklodowska Sq. 3, 20-031, Lublin, Poland.

Received: 23 December 2016 Accepted: 20 February 2017
Published online: 27 February 2017

References

1. Gao L, He J (2013) Surface hydrophobic co-modification of hollow silica nanoparticles toward large-area transparent superhydrophobic coatings. J Colloid Interface Sci 396:152–159
2. Ld F, Lottici PP, Lorenzi A, Montenero A, Salvioli-Mariani E (2011) Study of silica nanoparticles—polysiloxane hydrophobic treatments for stone-based monument protection. J Cult Heritage 12:356–363
3. Zhang X, Ye H, Xiao B, Yan L, Lv H, Jiang B (2010) Sol-gel preparation of PDMS/silica hybrid antireflective coatings with controlled thickness and durable antireflective performance. J Phys Chem C 114:19979–19983
4. Pinheiro AFM, Hoogendoorn D, Nijmeijer A, Winnubst L (2014) Development of a PDMS-grafted alumina membrane and its evaluation as solvent resistant nanofiltration membrane. J Membr Sci 463:24–32

5. Khanbabaei G, Vasheghani-Farahani E, Rahmatpour A (2012) Pure and mixed gas CH_4 and n-C_4H_{10} permeation in PDMS-fumed silica nanocomposite membranes. Chem Eng J 191:369–377. doi:10.1016/j.cej.2012.03.033
6. Cho YK, Park EJ, Kim YD (2014) Removal of oil by gelation using hydrophobic silica nanoparticles. J Ind Eng Chem 20(4):1231–1235. doi:10.1016/j.jiec.2013.08.005
7. Bolbukh Y, Terpiłowski K, Kozakevych R, Sternik D, Deryło-Marczewska A, Tertykh V (2016) Modified silicas with different structure of grafted methylphenylsiloxane layer. Nanoscale Res Lett 11(1):290. doi:10.1186/s11671-016-1513-7
8. Basu BJ, Kumar VD, Anandan C (2012) Surface studies on superhydrophobic and oleophobic polydimethylsiloxane–silica nanocomposite coating system. Appl Surf Sci 261:807–814
9. Cao R, Zhang X, Wu H, Wang J, Liu X, Jiang Z (2011) Enhanced pervaporative desulfurization by polydimethylsiloxane membranes embedded with silver/silica core-shell microspheres. J Hazard Mater 187(1–3):324–332. doi:10.1016/j.jhazmat.2011.01.031
10. Novotna P, Zita J, Krysa J, Kalousek V, Rathousky J (2007) Two-component transparent TiO_2/SiO_2 and TiO_2/PDMS films as efficient photocatalysts for environmental cleaning. Appl Catal B: Environmental 79:179–185. doi:10.1016/j.apcatb.2007.10.012
11. Ejenstam L, Swerin A, Pan J, Claesson PM (2015) Corrosion protection by hydrophobic silica particle-polydimethylsiloxane composite coatings. Corros Sci 99:89–97. doi:10.1016/j.corsci.2015.06.018
12. Harton SE, Templeman CG, Vylete B (2010) Percolation-driven multiscale roughening for superhydrophobic polymer nanocomposite coatings. Macromolecules 43:3173–3176. doi:10.1021/ma100044q
13. Klonos P, Sulym IY, Kyriakos K, Vangelidis I, Zidropoulos S, Sternik D, Borysenko MV, Kyritsis A, Deryło-Marczewska A, Gun'ko VM, Pissis P (2015) Interfacial phenomena in core-shell nanocomposites of PDMS adsorbed onto low specific surface area fumed silica nanooxides: effects of surface modification. Polymer 68:158–167
14. Klonos P, Kyritsis A, Pissis P (2015) Effects of surface modification and thermal annealing on the interfacial dynamics in core–shell nanocomposites based on silica and adsorbed PDMS. Eur Polym J 70:342–359. doi:10.1016/j.eurpolymj.2015.07.038
15. Sun S, Pan Z, Yang FK, Huang Y, Zhao B (2016) A transparent silica colloidal crystal/PDMS composite and its application for crack suppression of metallic coatings. J Colloid Interface Sci 461:136–143. doi:10.1016/j.jcis.2015.09.014
16. Klonos P, Kyritsis A, Bokobza L, Gun'ko VM, Pissis P (In Press, 2016) Interfacial effects in PDMS/titania nanocomposites studied by thermal and dielectric techniques. Colloids Surf A: Physicochemical and Engineering Aspects. 10.1016/j.colsurfa.2016.04.020
17. Klonos P, Dapei G, Sulym IY, Zidropoulos S, Sternik D, Deryło-Marczewska A, Borysenko MV, Gun'ko VM, Kyritsis A, Pissis P (2016) Morphology and molecular dynamics investigation of PDMS adsorbed on titania nanoparticles: effects of polymer molecular weight. Eur Polym J 74:64–80. doi:10.1016/j.eurpolymj.2015.11.010
18. Nakade M, Ogawa M (2007) Synthesis and characterization of zinc oxide fine particles coated with titania/PDMS hybrid. J Mater Sci 42:4254–4259. doi:10.1007/s10853-006-0672-9
19. Sötebier C, Michel A, Fresnais J (2012) Polydimethylsiloxane (PDMS) coating onto magnetic nanoparticles induced by attractive electrostatic interaction. Appl Sci 2:485–495. doi:10.3390/app2020485
20. Gun'ko VM, Borysenko MV, Pissis P, Spanoudaki A, Shinyashiki N, Sulim IY, Kulik TV, Palyanytsya BB (2007) Polydimethylsiloxane at the interfaces of fumed silica and zirconia/fumed silica. Appl Surf Sci 253:7143–7156
21. Kulyk K, Borysenko M, Kulik T, Mikhalovska L, Alexander JD, Palianytsia B (2015) Chemisorption and thermally induced transformations of polydimethylsiloxane on the surface of nanoscale silica and ceria/silica. Polym Degrad Stab 120:203–211
22. Galaburda MV, Klonos P, Gun'ko VM, Bogatyrov VM, Borysenko MV, Pissis P (2014) Dielectric properties and thermal destruction of poly(dimethylsiloxane)/Fe_2O_3/SiO_2 nanocomposites. Appl Surf Sci 305:67–76
23. Liu YL, Chen E (2010) Polymer crystallization of ultrathin films on solid substrates. Coord Chem Rev 254:1011–1037. doi:10.1016/j.ccr.2010.02.017
24. Schmidt DF, Giannelis EP (2010) Silicate dispersion and mechanical reinforcement in polysiloxane/layered silicate nanocomposites. Chem Mater 22:167–174. doi:10.1021/cm9026978
25. Wurm A, Ismail M, Kretzschmar B, Pospiech D, Schick C (2010) Retarded crystallization in polyamide/layered silicates nanocomposites caused by an immobilized interphase. Macromolecules 43:1480–1487. doi:10.1021/ma902175r
26. Akcora P, Liu H, Kumar SK, Moll J, Ki Y, Benicewicz BC, Linda SS, Acehan D, Panagiotopoulos AZ, Pryamitsyn V, Ganesan V, Ilavsky J, Thiyagarajan P, Colby RH, Douglas JF (2009) Anisotropic self-assembly of spherical polymer-grafted nanoparticles. Nature Materials 8:354–359. doi:10.1038/nmat2404
27. Harton SE, Kumar SK, Yang H, Koga T, Hicks K, Lee HK, Mijovic J, Liu M, Vallery RS, Gidley DW (2010) Immobilized polymer layers on spherical nanoparticles. Macromolecules 43:3415–3421. doi:10.1021/ma902484d
28. Rissanou AN, Harmandaris V (2014) Dynamics of various polymer–graphene interfacial systems through atomistic molecular dynamics simulations. Soft Matter 10:2876–2888. doi:10.1039/C3SM52688G
29. Vogiatzis GG, Theodorou DN (2014) Local segmental dynamics and stresses in polystyrene–C60 mixtures. Macromolecules 47:387–404. doi:10.1021/ma402214r
30. Fragiadakis D, Pissis P (2007) Glass transition and segmental dynamics in poly(dimethylsiloxane)/silica nanocomposites studied by various techniques. J Non-Cryst Solids 353:4344–4352. doi:10.1016/j.jnoncrysol.2007.05.183
31. Klonos P, Panagopoulou A, Bokobza L, Kyritsis A, Peoglos V, Pissis P (2010) Comparative studies on effects of silica and titania nanoparticles on crystallization and complex segmental dynamics in poly(dimethylsiloxane). Polymer 51:5490–5499. doi:10.1016/j.polymer.2010.09.054
32. Füllbrandt M, Purohit PJ, Schönhals A (2013) Combined FTIR and dielectric investigation of poly(vinyl acetate) adsorbed on silica particles. Macromolecules 46:4626–4632. doi:10.1021/ma400461p
33. Holt AP, Griffin PJ, Bocharova V, Agapov AL, Imel AE, Dadmun MD (2014) Dynamics at the polymer/nanoparticle interface in poly(2-vinylpyridine)/silica nanocomposites. Macromolecules 47:1837–1843. doi:10.1021/ma5000317
34. Sulym IY, Borysenko MV, Goncharuk O, Terpilowski K, Sternik D, Chibowski E (2011) Structural and hydrophobic–hydrophilic properties of nanosilica/zirconia alone and with adsorbed PDMS. Appl Surf Sci 258:270–277. doi:10.1016/j.apsusc.2011.08.045
35. Dyachenko AG, Borysenko MV, Pakhovchyshyn SV (2004) Hydrophilic/hydrophobic properties of silica surfaces modified with metal oxides and polydimethylsiloxane. Adsorpt Sci Technol 22:511–516. doi:10.1260/0263617042879546
36. Goncharuk OV, Sulym IY, Terpilowski K, Pakhlov EM (2015) Effect of the synthesis methods on hydrophobic properties of modified silicas. Adsorpt Sci Technol 33(6-8):709–714. doi:10.1260/0263-6174.33.6-8.709
37. Bergna HE (2005) Colloidal silica: fundamentals and applications. Taylor &Francis LLC, Salisbury
38. Legrand AP (1998) The surface properties of silicas. Wiley, New York
39. Iler RK (1979) The chemistry of silica. Wiley, Chichester
40. Voronkov M, Meleshkevich VP, Yuzhelevsky YA (1976) Siloxane bond. Nauka, Novosibirsk
41. Thomas S, Zaikov GE (2008) Polymer nanocomposite. Research Advances, Nova Publishers, USA
42. Sulym I, Sternik D, Oleksenko L, Lutsenko L, Borysenko M, Derylo-Marczewska A (2016) Highly dispersed silica-supported ceria–zirconia nanocomposites: preparation and characterization. Surf Interfaces 5:8–14. doi:10.1016/j.surfin.2016.08.001
43. Sulym I, Goncharuk O, Skwarek E, Sternik D, Borysenko MV, Derylo-Marczewska A, Janusz W, Gun'ko VM (2015) Silica-supported ceria–zirconia and titania–zirconia nanocomposites: structural characteristics and electrosurface properties. Colloids Surf A: Physicochemical and Engineering Aspects 482:631–638. doi:10.1016/j.colsurfa.2015.07.015
44. Law K-Y, Zhao H (2016) Surface wetting characterization, contact angle, and fundamentals. Springer International Publishing AG, Switzerland. doi:10.1007/978-3-319-25214-8
45. Terpiłowski K, Rymuszka D, Goncharuk OV, Sulym IY, Gun'ko VM (2015) Wettability of modified silica layers deposited on glass support activated by plasma. Appl Surf Sci 353:843–850
46. Goncharuk OV (2015) The heat of immersion of modified silica in polar and nonpolar liquids. J Therm Anal Calorim 120:1365–1373. doi:10.1007/s10973-015-4438-y
47. Takei T, Eriguchi E, Fuji M, Watanabe T, Chikazawa M (1998) Heat of immersion of amorphous and crystalline silicas in water: effect of crystallinity. Thermochim Acta 308:139–145
48. Gregg SJ, Sing KSW (1982) Adsorption, surface area and porosity. Academic, London

49. Gun'ko VM (2014) Composite materials: textural characteristics. Appl Surf Sci 307:444–454
50. Rymuszka D, Terpiłowski K, Hołysz L (2013) Influence of volume drop on surface free energy of glass. Annales UMCS Sectio AA 68:121–132
51. Chibowski E (2007) On some relations between advancing, receding and Young's contact angles. Adv Colloid Interf Sci 133:51–59
52. Kruk M, Jaroniec M (2001) Gas adsorption characterization of ordered organic–inorganic nanocomposite materials. Chem Mater 13:3169–3183, http://dx.doi.org/10.1021/cm0101069
53. Gun'ko VM, Turov VV (2013) Nuclear magnetic resonance studies of interfacial phenomena. CRC Press, Boca Raton
54. Kapridaki C, Maravelaki-Kalaitzaki P (2013) TiO_2–SiO_2–PDMS nano-composite hydrophobic coating with self-cleaning properties for marble protection. Prog Org Coat 76:400–410
55. Ren C, Qiu W, Chen Y (2013) Physicochemical properties and photocatalytic activity of the TiO_2/SiO_2 prepared by precipitation method. Separat Purifi Technol 107:264–272
56. Maji D, Lahirib SK, Das S (2012) Study of hydrophilicity and stability of chemically modified PDMS surface using piranha and KOH solution. Surf Interf Anal 44:62–69. doi:10.1002/sia.3770
57. Adamson AW, Gast AP (1997) Physical chemistry of surfaces, 6th edn. Wiley, New York
58. Van OCJ, Chaudhury MK, Good RJ (1988) Interfacial Lifshitz-van der waals and polar interactions in macroscopic systems. Chem Rev 88:927–941
59. Somasundaran P (2006) Encyclopedia of surface and colloid science (1). CRC Press, Boca Raton
60. Melrose JC (1967) Immersion heat relationships for homogeneous surfaces. J Colloid Interface Sci 24:416–426